HHS Public Access

Author manuscript

Neural Comput. Author manuscript; available in PMC 2018 July 04.

Published in final edited form as:

Neural Comput. 2018 July ; 30(7): 1725–1749. doi:10.1162/neco_a_01087.

Joint Estimation of Effective BrainWave Activation Modes using EEG/MEG Sensor Arrays and Multi-modal MRI Volumes

Vitaly L. Galinsky[1,4], **Antigona Martinez**[5,6], **Martin P. Paulus**[7], and **Lawrence R. Frank**[1,2,3]

[1]Center for Scientific Computation in Imaging, University of California at San Diego, La Jolla, CA 92093-0854, USA

[2]Department of Radiology, University of California at San Diego, La Jolla, CA 92093-0854, USA

[3]VA San Diego Healthcare System, San Diego, CA 92161, USA

[4]Electrical and Computer Engineering Department, University of California at San Diego, La Jolla, CA 92093-0407, USA

[5]Division of Experimental Therapeutics, Department of Psychiatry, Columbia University, New York, NY 10032, USA

[6]Schizophrenia Research Division, Nathan Kline Institute for Psychiatric Research, Orangeburg, NY 10962, USA

[7]Laureate Institute for Brain Research, Tulsa, OK 74136-3326, USA

Abstract

In this paper we present a new method for integration of sensor-based multi-frequency bands of EEG and MEG datasets into a voxel-based structural-temporal MRI analysis by utilizing the general *Joint ESTimation using Entropy Regularization* (**JESTER**) framework. This allows the enhancement of the spatial-temporal localization of brain function and the ability to relate it to morphological features and structural connectivity. This method has broad implications for both basic neuroscience research and clinical neuroscience focused on identifying disease-relevant biomarkers by enhancing the spatial-temporal resolution of the estimates derived from current neuroimaging modalities thereby providing a better picture of the normal human brain in basic neuroimaging experiments and variations associated with disease states.

Keywords

Magnetic Resonance Imaging; Diffusion MRI; Functional MRI; EEG; MEG

1 Introduction

Three cutting-edge technologies have emerged as the primary non-invasive functional neuroimaging modalities for studying the human brain: functional magnetic resonance imaging (FMRI), electroencephalography (EEG), and magnetoen-cephalography (MEG) (Churchland & Sejnowski, 1988). Each of these provides unique information but at different spatial and temporal scales and thus have their own strengths and weaknesses. The measured signal changes in FMRI are related to changes in blood oxygenation (Buxton & Frank,

1997) and are thus only indirectly related to neural activity and occur on a very slow time scale ($\approx 1s$). EEG and MEG, on the other hand, capture the direct effects of neural activity with exquisite temporal resolution ($\approx 1ms$), but with very poor spatial resolution and can only measure activity in the cortex because electrical/magnetic fields decay rapidly with distance, whereas MRI can detect activity throughout the entire brain with excellent spatial resolution ($\approx 1mm$).

The ability to leverage the strengths of these different acquisition modalities by combining their analysis into a single framework would thus have the potential to produce estimates of structure-function relationships in the brain with greater spatial-temporal resolution than any of these methods taken individually. This potential advantage of multimodal integration of EEG, MEG and neuro-MRI signals is well recognized and has been actively pursued in the last two decades using a range of analysis approaches ranging from simultaneous EEG/MRI acquisition to reconstruction algorithms that model the neuronal generators of EEG/MEG potentials based on FMRI activations obtained under the same task parameters (Sommer et al., 2003; Singh et al., 2002; Vanni et al., 2004). However, current approaches typically rely on a set of restrictive assumptions and combined with numerous conceptual and methodological challenges, the ability to fully combine modalities for the purpose of non-invasive study of human brain structure-function relationships remains an elusive capability.

This problem of combining multiple imaging modalities is ubiquitous across a wide range of scientific fields. In fact, it is an important problem in neuroimaging with MRI (neuro-MRI) where the three primary methods - high spatial resolution anatomical data (HRA), diffusion tensor imaging (DTI), and functional MRI, (either resting state, rsFMRI, or task-based), provide multivariate information on, respectively, brain morphology, neural connectivity, and brain activity at different spatial and temporal resolutions. To address this problem, we have recently developed a theoretical and computational framework for *Joint ESTimation using Entropy Regularization* (**JESTER**) (Galinsky & Frank, 2017b) of the structural and functional parameters provided by these modalities, using each to constrain the others and thus significantly improving the veracity of the estimation procedure. The approach employs probabilistic framework to generate both intra- and inter- modality coupling in a consistent manner expressed through the *entropy spectrum pathways* (**ESP**) (Frank & Galinsky, 2014). The JESTER method integrates three approaches that we developed for separately analyzing each modality: 1) *Spherical wave decomposition* (**SWD**) (Galinsky & Frank, 2014) for shape analysis and segmentation of HRA data; 2) *Geometrical optics guided by entropy spectrum pathways (***GO-ESP***)* (Frank & Galinsky, 2014; Galinsky & Frank, 2015) for simultaneous estimation of local diffusion and global tractography from DTI data; 3) *Entropy field decomposition* (**EFD**) (Frank & Galinsky, 2016a, b) for characterization and estimation of space-time brain activation patterns from resting-state FMRI data (**rsFMRI**); in conjunction with a new non-linear registration method (**SYM-REG**) (Galinsky & Frank, 2017b, a) capable of robustly and efficiently combining multi-modal and multi-subject data.

From a pure terminology perspective, in this paper the EFD will refer to a procedure for extraction of a sequence of spatio-temporal patterns (activation modes) from single modality space-time volume. And an extension of EFD procedure that employs a combination of

multiple MRI modalities (with the help of SWD and GO-ESP) for each spatial location will be referred to as the JESTER method.

It is important to emphasize that the JESTER framework is very general, may be used with data of different structure and extent, including scalar, vector, tensorial or time-series multi-dimensional data, and is not specific to MRI. In this paper we expanded its capabilities by incorporating both EEG and MEG with the three MRI modalities to enhance the spatial-temporal localization of brain function and relate it to morphological features and structural connectivity. This enhanced version of JESTER to incorporate cortical electrophysiological measurements is called **CORT-JESTER**.

2 Method

In order to be able to include EEG/MEG datasets into our joint estimation scheme we first need to develop an approximation for the volumetric distribution of electrostatic potential inside the MRI domain. In a most general form this approximation can be derived using Maxwell equations in a medium. Nevertheless, this is inherently ill–posed inverse problem that requires regularization and available multi-modal MRI volumes can be used as constraints to restrict a space of available solutions.

2.1 Theory

Brain electromagnetic activity can be described using Gauss's and Ampere's laws from macroscopic Maxwell equations

$$\nabla \cdot \mathbf{D} = \rho,$$
$$\nabla \times \mathbf{H} = \mathbf{J} + \frac{\partial \mathbf{D}}{\partial t},$$

where $\mathbf{D}(t, \mathbf{x})$ is the displacement field and $\mathbf{H}(t, \mathbf{x})$ is the magnetizing field. The source terms in these equations include a density of free charges $\rho(\mathbf{x})$ and a free current density $\mathbf{J}(\mathbf{x})$. We will assume linear electrostatic and magnetostatic properties of the brain tissues, i.e. use the relations $\mathbf{D}_\omega = \varepsilon \mathbf{E}_\omega$, $\mathbf{H}_\omega = 1/\mu \mathbf{B}_\omega$, where $\mathbf{E}(t, \mathbf{x})$ is the electric field, $\mathbf{B}(t, \mathbf{x})$ is the magnetic field, and ε and μ are the permittivity and permeability coefficients, that may depend on the frequency ω.

Alternatively, both of these equations can be expressed in the form of a single charge continuity equation:

$$\frac{\partial \rho}{\partial t} + \nabla \cdot \mathbf{J} = 0$$

Using electrostatic potential ϕ ($\mathbf{E} = -\nabla\phi$) and Ohm's law $\mathbf{J} = \boldsymbol{\Sigma} \cdot \mathbf{E}$, the charge continuity equation can be rewritten as

$$\frac{\partial}{\partial t}(\nabla \cdot \varepsilon \nabla \phi) + \nabla \cdot \boldsymbol{\Sigma} \cdot \nabla \phi = 0, \quad (1)$$

where $\boldsymbol{\Sigma} = \{\Sigma^{ij}\}$ is a local tissue conductivity tensor. Taking the temporal Fourier transform (i.e. replacing $\partial/\partial t \rightarrow -I\omega$, $I^2 = -1$), this can be written in tensor form as

$$(\Sigma^{ij} - I\omega\varepsilon\delta^{ij})\,\partial_i\partial_j\phi_\omega = \left[I\omega(\partial_i\varepsilon)\delta^{ij} - (\partial_i\Sigma^{ij})\right]\partial_j\phi_\omega, \quad (2)$$

where a summation is assumed over repeated indices.

Rearranging the above expression to separate the isotropic and homogeneous terms gives

$$\hat{L}\phi_\omega = \hat{R}\phi_\omega \quad (3)$$

written in terms of the operators

$$\hat{L} \equiv \partial^i\partial_i$$
$$\hat{R} \equiv \frac{\sigma + I\omega\varepsilon}{\sigma^2 + \omega^2\varepsilon^2}\left[I\omega(\partial_i\varepsilon)\delta^{ij} - (\partial_i\Sigma^{ij}) - (\Sigma^{ij} - \sigma\delta^{ij})\,\partial_i\right]\partial_j,$$

where σ is an isotropic local conductivity $\sigma = Tr\Sigma/3 = \sum_i^i/3$. Terms in square brackets show that the parts of $\hat{R}\phi_\omega$ can be interpreted in terms of different tissue characteristics and may be important for understanding the origin of sources of the electro-/magnetostatic signal detected by the EEG/MEG sensors. The first term ($\omega(\partial^i\varepsilon)(\partial_i\phi_\omega)$) corresponds to areas with sudden change in permittivity, e.g. the white-gray matter interface. The second term (($\partial_i\Sigma^{ij}$)($\partial_j\phi_\omega$)) corresponds to regions where the conductivity gradient is the strongest, i.e. the gray matter/CSF boundary. Finally, the last term ($\Sigma^{ij}\partial_i\partial_j\phi_\omega - \sigma\partial^i\partial_i\phi_\omega$) includes areas with the strongest conductivity anisotropies, e.g. input from major white matter tracts.

2.2 Inverse Solution

For this paper it is assumed that we have the three standard neuro-MRI acquisitions (HRA, DTI, rsFMRI). The data from these modalities can be used to constrain the values of $\boldsymbol{\Sigma}$ and ε. The DTI data allows the construction of estimates of the conductivity tensor anisotropy, whereas HRA and rsFMRI data is useful for tissue segmentation and assignment of mean values for permittivity and conductivity (see table 1).

An approximate solution for the potential ϕ across an entire MRI brain volume can be constructed iteratively as

$$\hat{L}\phi_{\omega}^{(k)} = \hat{R}\phi_{\omega}^{(k-1)} \quad (4)$$

$$\tilde{\phi}_{\omega}^{(K)} = \alpha_K \sum_{k=0}^{K} \phi_{\omega}^{(k)} \quad (5)$$

where single iteration forward solution can be found either by using the Green function $G(\mathbf{x}, \mathbf{x}') = 1/(4\pi|\mathbf{x} - \mathbf{x}'|)$ or by applying a Fourier-space pseudospectral approach (Gottlieb & Orszag, 1977).

We should emphasize that the use of a pseudospectral approach provides a number of important advantages over finite/boundary element (FEM/BEM) approaches most commonly performed for electrostatic modeling of brain activity (Gramfort et al., 2010; Kybic et al., 2005; von Ellenrieder et al., 2009; Gutierrez & Nehorai, 2008; Schimpf et al., 2002; Ermer et al., 2001; Mosher et al., 1999). The pseudospectral formulation does not use surface meshes and as a consequence, does not require limiting the location of sources by a single surface (or small number of surfaces) with fixed number of surface pinned static dipole sources. This is also true for target locations, as typically FEM/BEM approaches obtain the solution only at a small number of fixed position sensors. The pseudospectral approach is able to find a time dependent spatial distribution of electrostatic potential at every space-time location of multidimensional volume as a superposition of source inputs from every voxel of the same volume. The forward solution for the electrostatic potential ϕ can be constructed through a direct summation, i.e. using static Green function and restricting the number of sources/targets by a selected set of mesh locations, thus obtaining something equivalent to a FEM/BEM solver. Alternatively, it can be obtained as a sum of inputs from all spatial and temporal Fourier modes using frequency/wave number domain for description of both a Green function and volume distribution of sources, resulting in pseudo-spectral formulation (where the use of fast Fourier transform permits effective numerical implementation). This approach includes the distribution of both electrostatic and geometric properties of the media (conductivity, permittivity, anisotropy, inhomogeneity) at every location throughout the volume (that is guided by MRI acquisition and analysis), therefore, it models wave-like signal propagation inside the volume and should be able to describe and uncover significantly more complex dynamical behavior of the sources of the electrostatic activity recorded at the sensor locations. To illustrate this and show some examples of this complex activity we included in Figures 1 and 2 hyperlinks to videos of the space-time variations resulted from some rsFMRI modes used as space-time sources.

An array of EEG sensors at locations $\mathbf{x}^{(n)}$, $n = 1..N$ can be used to constrain the solution and find coefficients α_K by minimizing the deviation functional

$$\mathcal{R}_{\Delta}^{(k)} = \min\left(\sum_{n=1}^{N}\left[\Phi_{\omega}^{(n)} - \tilde{\phi}_{\omega}^{(K)}\left(\mathbf{x}^{(n)}\right)\right]^2\right) \quad (6)$$

with an additional requirement that an approximation error $\mathcal{R}_{\Delta}$ is bounded by a chosen accuracy ε

$$\mathcal{R}_{\Delta}^{(K)} \equiv \alpha_K^2\left\|\phi_{\omega}^{(K)}\right\| \leq \varepsilon \Rightarrow \alpha_K^2 \leq \varepsilon / \left\|\phi_{\omega}^{(K)}\right\|, \quad (7)$$

where $\Phi_{\omega}^{(n)}$ is a potential at frequency ω detected by the sensor n. The iterations will be stopped if the convergence cannot be achieved (i.e. $\mathcal{R}_{\Delta}^{(K)} > \mathcal{R}_{\Delta}^{(K-1)}$). As an initial approximation $\phi_{\omega}^{(0)}$ any appropriate fit to Eqn 6 can be used that satisfies $\partial^i \partial_i \phi_{\omega}^{(0)} = 0$, e.g. a linear function of coordinates $\phi_{\omega}^{(0)} = \beta_i x_i + \gamma$ with coefficients β_i determined from the least square fit Eqn 6.

This approach for finding an inverse solution can be applied to an array of MEG sensors without any modifications except a difference in a form of the deviation functional, where instead of an electrostatic potential $\tilde{\phi}_{\omega}^{(K)}$ at sensor location $\mathbf{x}^{(n)}$, either magnetic flux or the projection of its gradient should be substituted for either magnetometers or gradiometers respectively (both quantities can be derived from free vacuum form of Maxwell equations).

2.3 Wave Activation Modes

The potential $\tilde{\phi}_{\omega}^{(K)}$ Eqn 5 is the central quantity that will be used to derive various measures. It can be calculated over arbitrary frequency ranges $\omega = \omega_1 \ldots \omega_2$ and thus it is possible to calculate it over the standard alpha, beta, and delta bands (or any parts or combinations of them) typically identified in EEG. These potentials can then be converted to the time domain $\tilde{\phi}(t, \mathbf{x})$ and used for EFD analysis (Frank & Galinsky, 2016a, b) generating time-space brain activation modes ranked by the power. Alternatively, the estimated potentials $\tilde{\phi}(t, \mathbf{x})$ can be used in joint estimation scheme presented in Galinsky & Frank (2017a) as an additional modality Q_{ij}^E in the intermodality coupling matrix Q_{ij}, resulting in cortically electrophysiologically enhanced version of JESTER (or CORT-JESTER) that can provide significant time resolution improvement over low frequency FMRI data.

The details of the mathematical formulation of EEG/MEG specific coupling matrix Q_{ij}^E as well as a short summary of JESTER are included in the Appendix.

2.4 Computational Implementation

The multi-sensor EEG and multi-modal MRI data were used for coupling by generation of frequency dependent inverse Green function for every voxel inside the high resolution MRI

domain using multiple layer classification of head tissues (GM, WM, CSF, scalp and skull, see table 1) with the spherical wave decomposition (SWD) (Galinsky & Frank, 2014) based segmentation of the HRA T1 volumes.

The processing of both resting state and task-based EEG datasets HRA, DTI, and rsFMRI datasets involves the following steps:

1. Segmentation of anatomical datasets using the SWD including skull stripping and gray/white matter extraction;
2. Registration of DTI and rsFMRI datasets with the HRA dataset and extraction of functionally active modes (regions) of the brain;
3. Generation of anisotropy conductivity tissue maps from DTI data;
4. Generation of inhomogeneous permittivity tissue maps (that is effectively restricting possible source areas for the EEG activity) using a combination of rsFMRI activation modes and HRA/DTI gray matter, including anisotropy estimation;
5. Generation of a frequency dependent inverse Green function for each EEG recorded frequency and solving for $\tilde{\phi}_{\omega}^{(K)}$ (Eqn 5) that includes MRI based regularization constraints;
6. Generation of FMRI-like volumes of signal time courses in each voxel for various EEG bands (including a low frequency FMRI-like range, as well as the standard alpha, beta and delta bands);
7. Extraction of space-time modes from FMRI-like EEG volumes using the JESTER procedure.

3 Results and Discussion

3.1 Data

Several independent sources of MRI, EEG and MEG datasets were used for testing and validation of the CORT-JESTER algorithms. The variety of selected datasets allows to target different aspects of algorithm performance. This may include assessment of mode repeatability and both intra and inter subject similarity for different subjects, sessions and stimuli, assessment of importance and effects of different modalities in simultaneous EEG/rsFMRI acquisitions, comparison of modes between EEG and MEG, etc. Some of these datasets are publicly accessible and available from the open source Human Connectome Project (Van Essen et al., 2013, 2012; Sotiropoulos et al., 2013), and include the HRA T1 volumes, the DTI volumes, as well as resting state and task based FMRI and MEG acquisitions (CONNECTOME-D). The HCP datasets were collected on the customized Siemens 3T Connectom scanner, which is a modified 3T Skyra system (MAGNETOM Skyra Siemens Healthcare), housed at the MGH/HST Athinoula A. Martinos Center for Biomedical Imaging (see Setsompop et al. (2013) for details of the scanner design and implementation). A 64-channel, tight-fitting brain array coil (Keil et al., 2013) was used for data acquisition. The dataset contains 96 slices of 140×140 matrix (1.5 mm linear voxel size)

at four levels of diffusion sensitizations (b-values b=1k, 3k, 5k and 10k s/mm^2) distributed over 552 total q-vectors. HCP MEG data acquisition was performed on a whole head MAGNES 3600 (4D Neuroimaging, San Diego, CA) system housed in a magnetically shielded room, located at the Saint Louis University (SLU) medical campus. The sampling rate was selected to be as high as possible (2034.51 Hz) while collecting all channels (248 magnetometer channels together with 23 reference channels). Bandwidth was set (at DC, 400Hz) to capture physiological signals

Several HRA, DTI and rsFMRI datasets were collected locally at the UCSD Center for Functional MRI (CFMRI). The CFMRI data were acquired with a 3T GE Discovery MR750 whole body system (CFMRI-D). The anatomical T1 volumes have 168×256×256 voxel size with 1.2×0.9375×0.9375mm^3 resolution. A multiband DTI EPI acquisition (Setsompop et al., 2011) developed at the CFMRI employed three simultaneous slice excitations to acquire data with three diffusion sensitizations (at b-values b=1000/2000/3000 s/mm^2) for 30, 45 and 65 different diffusion gradients (respectively) uniformly distributed over a unit sphere. Several baseline (b=0) images were also recorded. The data were reconstructed offline using the CFMRI's multiband reconstruction routines. The DWI datasets have 100×100×72 matrix size with 2×2×2mm^3 resolution. Whole brain BOLD resting-state data were acquired over thirty axial slices using an echo planar imaging (EPI) sequence (flip angle = 70°, slice thickness=4mm, slice gap=1mm, FOV=24cm, TE= 30 ms, TR = 1.8 s, matrix size = 64×64×30). Further details are available in Wong et al. (2013). All data were pre-processed using the standard pre-processing analysis pathway at the CFMRI (as described in Wong et al. (2013)). Nuisance terms were removed from the resting-state BOLD time series through multiple linear regression. These nuisance regressors included: i) linear and quadratic trends, ii) six motion parameters estimated during image co-registration and their first derivatives, iii) RETROICOR (2nd order Fourier series) (Glover et al., 2000) and RVHRCOR (Chang & Glover, 2009) physiological noise terms calculated from the cardiac and respiratory signals, and iv) the mean BOLD signals calculated from white matter and CSF regions and their first respective derivatives, where these regions were defined using partial volume thresholds of 0.99 for each tissue type and morphological erosion of two voxels in each direction to minimize partial voluming with gray matter.

For EEG and same subject MRI CORT-JESTER testing and validation several datasets from two unrelated studies were used.

The first study concentrated on detection of effects of medication on the resting state EEG and FMRI. All the datasets for this study were collected at the Laureate Institute for Brain Research (Zotev et al., 2016) and include simultaneously acquired EEG and rsFMRI recordings at 4ms for 500s as well as HRA T1 volumes (LIBR-D). Additionally, these simultaneous EEG and rsFMRI acquisitions for each subject were repeated tree times. The clinical results for this study will be reported elsewhere. In this paper we used these simultaneous and repeated EEG and rsFMRI acquisitions to study repeatability of the CORT-JESTER approach.

The second set of multimodal (EEG and MRI) datasets was acquired by the Javitt Group in Nathan Kline Institute for Psychiatric Research (Javitt, 2009; Javitt & Sweet, 2015). The

data includes task and resting state EEG and FMRI recordings at 2ms for about 30min total and HRA T1 volumes (NKIPR-D). The task based EEG and FMRI datasets contain several acquisitions of response for similar stimuli that can be used for test-retest purposes. Again the clinical results for this study will be reported elsewhere.

3.2 FMRI Modes as EEG Sources

Functional modes (Frank & Galinsky, 2016b) estimated from rsFMRI (CFMRI-D) with JESTER (Galinsky & Frank, 2017b) show the brain's functional organization and functional connectivity through a number of consistent networks at different stages of consciousness and thus represent specific patterns of synchronous activity. This synchronism can be assumed to be related to different space-time sources of electrophysiological activity. Therefore, we can use those modes to find what low frequency response they will generate at EEG/MEG sensor positions. Several examples of generated space-time distributions of the electric fields at the skull and at the cortex are shown in Figure 1 and Figure 2 with embedded and hyperlinked videos of the space-time variations.

3.3 MEG Data

MEG datasets (CONNECTOME-D) with relatively large number of sensors comparing to EEG (248 magnetometer and 23 reference channels vs 32 or 64 head sensors and 1 reference) allow to obtain detailed space-time wave activity modes. Several examples of these modes are shown in Figure 3. The high resolution anatomical and diffusion weighted datasets were used for tissue classification and assignment of electro/magneto-static properties for each voxel. Selected at random activation modes include bilateral anterior insula, which is among the most common activation patterns in rsFMRI as well as the area that is most commonly dysfunctional in psychiatric disorders (Goodkind et al., 2015), right caudate, and medial frontal gyrus.

No rsFMRI data was used for the CONNECTOME-D analysis. Generally speaking, the combination of rsFMRI spatial activation modes and and HRA/DTI gray matter estimations is used only for setting the volumetric inhomogeneous distribution of permittivity. That is, rsFMRI modes can only constrain source regions indirectly by their influence in shaping the volumetric permittivity distribution. The additional information that rsFMRI provides is expected to result in a relatively small (may be even marginal) overall improvement, due to low resolution. Nevertheless, even without the use of rsFMRI modes, the MEG activation patterns in Figure 3 still shows patterns which are among the most common activation patterns observed by rsFMRI.

3.4 EEG Data

The first set of EEG data (LIBR-D) was recorded with relatively sparse spatial array of sensors (32 head sensors plus 1 reference) with temporal resolution of 4ms. The data acquisition was completed during a rest state without task based stimuli simultaneously with acquisition of functional MRI volumes. For each subject three recording sessions were conducted. The CORT-JESTER procedure was used to generate a new volume for each EEG set with the same spatial and temporal resolution as the FMRI dataset (2mm × 2mm × 2mm × 2s and 80 × 95 × 75 voxels with 237 time points). Each volume was then used in EFD

procedure to generate activation modes in the same way it is done for FMRI volumes. Figure 4 shows two randomly selected modes for two subjects for all three sessions. Both subjects and modes show very good mode similarity between sessions and at the same time some noticeable subject differences. To quantitatively evaluate mode repeatability we used the intraclass correlation coefficient (Sokal & Rohlf, 1995) (ICC) calculated as a ratio of variance across mode groups to the total variance. For two mode groups shown in Figure 4 the ICC is equal to 0.9985. For several other mode groups (not shown) ICC values from 0.9 to 0.99 and higher were obtained.

The LIBR-D set includes simultaneously acquired EEG and FMRI volumes (both task based and resting state) and potentially allows to conduct a study of correspondence between EEG and FMRI. This is clearly a very important question and a number of studies have appeared recently that focus on simultaneous acquisition techniques and provide attempts to confirm (or rebuff) the existence of correlations between EEG and FMRI data at different frequency bands or under different acquisition conditions (Meyer, van Oort, & Barth, 2013; Musso et al., 2010; Fellner et al., 2016; Meyer, Janssen, et al., 2013; Chang et al., 2013; Mantini et al., 2007). While we agree that the question of FMRI-EEG concordance is important, the complexity of the subject, and proving or disproving existence of the EEG-rsFMRI concordance, is clearly beyond the scope of our paper. We would like to emphasize that the main purpose of our paper is to devise a method for use of complementary features from EEG and FMRI modalities (Allen et al., 2018), e.g. difference in temporal and spatial resolution, to enhance estimation of brain activation modes.

Figure 5 shows several EEG functional modes generated for alpha band using higher spatial resolution (the same resolution as in HRA acquisition, 1mm×1mm× 1mm and 161×191×151 voxels with 237 time points)

The second set of EEG data (NKIPR-D) was recorded with higher number of sensors (64 head sensors plus 1 reference) and with higher temporal resolution as well (2ms). The data acquisition included both resting state and stimuli for various tasks. Figure 6 shows several EEG functional modes generated for alpha band task stimuli (the spatial resolution from HRA volume is 1mm×1mm×1mm and 192×256×256 voxels and the number of time points is 123). The modes show very good similarity between similar stimuli in each subject.

4 Conclusions

We presented an extension of the theory for the joint estimation of the structural-functional brain modes, that have been initially applied to the three primary neuro-MRI modalities - high resolution anatomical (HRA) data, diffusion tensor imaging (DTI) data, and resting state functional MRI (rsFMRI) data, to include high temporal resolution EEG and EEG modalities.

Joint estimation refers to estimation of activation modes that includes (as a first step) the EEG time course reconstruction at each voxel location using EM parameters estimated from the various modalities of MRI, followed by the multimodal activation mode estimation that includes a combination of both MRI and EEG/MEG modalities.

We applied the method to multi-modal MRI/EEG/MEG resting and task–based dataset showing good repeatability and similarity between subjects, with the intraclass correlation coefficient ranging from 0.9 to higher than 0.99. This method may potentially have broad implications for both basic neuroscience and clinical studies by enhancing the spatial-temporal resolution of the estimates derived from current neuroimaging modalities thereby providing a better picture of the normal human brain in basic neuroimaging experiments and variations associated with disease states.

Acknowledgments

The authors thank Dr Alec Wong and Dr Tom Liu at the UCSD CFMRI for providing the resting state data and Dr Scott Sorg at the VA San Diego Health Care System for providing the diffusion weighted imaging data. LRF and VLG were supported by NSF grants DBI-1143389, DBI-1147260, EF-0850369, PHY-1201238, ACI-1440412, ACI-1550405 and NIH grant R01 MH096100. Data were provided [in part] by the Human Connectome Project, WU-Minn Consortium (Principal Investigators: David Van Essen and Kamil Ugurbil; 1U54MH091657) funded by the 16 NIH Institutes and Centers that support the NIH Blueprint for Neuroscience Research; and by the McDonnell Center for Systems Neuroscience at Washington University. Data collection and sharing for this project was provided by the Human Connectome Project (HCP; Principal Investigators: Bruce Rosen, M.D., Ph.D., Arthur W. Toga, Ph.D., Van J. Weeden, MD). HCP funding was provided by the National Institute of Dental and Craniofacial Research (NIDCR), the National Institute of Mental Health (NIMH), and the National Institute of Neurological Disorders and Stroke (NINDS). HCP data are disseminated by the Laboratory of Neuro Imaging at the University of Southern California.

References

Allen EA, Damaraju E, Eichele T, Wu L, Calhoun VD. EEG Signatures of Dynamic Functional Network Connectivity States. Brain Topogr. 2018 Jan; 31(1):101–116. [PubMed: 28229308]

Burda Z, Duda J, Luck J, Waclaw B. Localization of the maximal entropy random walk. Phys Rev Lett. 2009; 102(16):160602. [PubMed: 19518691]

Buxton RB, Frank LR. A model for the coupling between cerebral blood flow and oxygen metabolism during neural stimulation. J Cerebr Blood Flow Metab. 1997; 17(1):64–72.

Chang C, Glover GH. Effects of model-based physiological noise correction on default mode network anti-correlations and correlations. Neuroimage. 2009; 47(4):1448–1459. [PubMed: 19446646]

Chang C, Liu Z, Chen MC, Liu X, Duyn JH. EEG correlates of time-varying BOLD functional connectivity. Neuroimage. 2013 May.72:227–236. [PubMed: 23376790]

Churchland PS, Sejnowski TJ. Perspectives on cognitive neuroscience. Science. 1988 Nov; 242(4879): 741–745. [PubMed: 3055294]

Enßlin TA, Frommert M, Kitaura FS. Information field theory for cosmological perturbation reconstruction and nonlinear signal analysis. Phys Rev D. 2009 Nov.80(10):105005.

Ermer JJ, Mosher JC, Baillet S, Leah RM. Rapidly recomputable EEG forward models for realistic head shapes. Phys Med Biol. 2001 Apr; 46(4):1265–1281. [PubMed: 11324964]

Fellner MC, Volberg G, Mullinger KJ, Goldhacker M, Wimber M, Greenlee MW, Hanslmayr S. Spurious correlations in simultaneous EEG-fMRI driven by in-scanner movement. Neuroimage. 2016 Jun.:133.

Feynman RP. Space-time approach to quantum electrodynamics. Phys Rev. 1949; 76(6):769–789.

Frank LR, Galinsky VL. Information pathways in a disordered lattice. Phys Rev E. 2014; 89(3):11.

Frank LR, Galinsky VL. Detecting spatio-temporal modes in multivariate data by entropy field decomposition. J Phys A. 2016a; 49:395001.

Frank LR, Galinsky VL. Dynamic multi-scale modes of resting state brain activity detected by entropy field decomposition. Neural Comput. 2016b; 28(9):1769–1811. [PubMed: 27391678]

Gabriel S, Lau RW, Gabriel C. The dielectric properties of biological tissues: III. Parametric models for the dielectric spectrum of tissues. Phys Med Biol. 1996a Nov; 41(11):2271–2293. [PubMed: 8938026]

Gabriel S, Lau RW, Gabriel C. The dielectric properties of biological tissues: II. Measurements in the frequency range 10 Hz to 20 GHz. Phys Med Biol. 1996b Nov; 41(11):2251–2269. [PubMed: 8938025]

Galinsky VL, Frank LR. Automated segmentation and shape characterization of volumetric data. Neuroimage. 2014; 92:156–168. [PubMed: 24521852]

Galinsky VL, Frank LR. Simultaneous multi-scale diffusion estimation and tractography guided by entropy spectrum pathways. IEEE Trans Med Imag. 2015 May; 34(5):1177–1193.

Galinsky VL, Frank LR. Symplectomorphic registration with phase space regularization by entropy spectrum pathways. IEEE Med Image Anal. 2017a in review.

Galinsky VL, Frank LR. A unified theory of neuro-MRI data shows scale-free nature of connectivity modes. Neural Comput. 2017b Jan. (accepted).

Glover GH, Li TQ, Ress D. Image-based method for retrospective correction of physiological motion effects in fMRI: RETROICOR. Magn Reson Med. 2000; 44(1):162–167. [PubMed: 10893535]

Goodkind M, Eickhoff SB, Oathes DJ, Jiang Y, Chang A, Jones-Hagata LB, … Etkin A. Identification of a common neurobiological substrate for mental illness. JAMA Psychiatry. 2015 Apr; 72(4):305–315. [PubMed: 25651064]

Gottlieb, D., Orszag, S. Numerical analysis of spectral methods. Society for Industrial and Applied Mathematics; 1977. Retrieved from http://epubs.siam.org/doi/abs/10.1137/1.9781611970425

Gramfort A, Papadopoulo T, Olivi E, Clerc M. OpenMEEG: opensource software for quasistatic bioelectromagnetics. Biomed Eng Online. 2010 Sep.9:45. [PubMed: 20819204]

Gutierrez D, Nehorai A. Array response kernels for EEG and MEG in multilayer ellipsoidal geometry. IEEE Trans Biomed Eng. 2008 Mar; 55(3):1103–1111. [PubMed: 18334402]

Javitt DC. When doors of perception close: Bottom-up models of disrupted cognition in schizophrenia. Annu Rev Clin Psychol. 2009; 5:249–275. [PubMed: 19327031]

Javitt DC, Sweet RA. Auditory dysfunction in schizophrenia: Integrating clinical and basic features. Nat Rev Neurosci. 2015; 16(9):535–550. [PubMed: 26289573]

Jaynes E. Information Theory and Statistical Mechanics. Physical Review. 1957a; 106(4):620–630.

Jaynes E. Information theory and statistical mechanics. II. Physical Review. 1957b; 108(2):171.

Keil B, Blau JN, Biber S, Hoecht P, Tountcheva V, Setsompop K, … Wald LL. A 64-channel 3t array coil for accelerated brain mri. Magn Reson Med. 2013; 70(1):248–258. [PubMed: 22851312]

Kybic J, Clerc M, Abboud T, Faugeras O, Keriven R, Papadopoulo T. A common formalism for the integral formulations of the forward EEG problem. IEEE Trans Med Imaging. 2005 Jan; 24(1):12–28. [PubMed: 15638183]

Mantini D, Perrucci MG, Del Gratta C, Romani GL, Corbetta M. Electrophysiological signatures of resting state networks in the human brain. Proc Natl Acad Sci USA. 2007 Aug; 104(32):13170–13175. [PubMed: 17670949]

Meyer MC, Janssen RJ, Van Oort ES, Beckmann CF, Barth M. The Quest for EEG Power Band Correlation with ICA Derived fMRI Resting State Networks. Front Hum Neurosci. 2013; 7:315. [PubMed: 23805098]

Meyer MC, van Oort ES, Barth M. Electrophysiological correlation patterns of resting state networks in single subjects: a combined EEG-fMRI study. Brain Topogr. 2013 Jan; 26(1):98–109. [PubMed: 22752947]

Mosher JC, Leahy RM, Lewis PS. EEG and MEG: forward solutions for inverse methods. IEEE Trans Biomed Eng. 1999 Mar; 46(3):245–259. [PubMed: 10097460]

Musso F, Brinkmeyer J, Mobascher A, Warbrick T, Winterer G. Spontaneous brain activity and EEG microstates. A novel EEG/fMRI analysis approach to explore resting-state networks. Neuroimage. 2010 Oct; 52(4):1149–1161. [PubMed: 20139014]

Schimpf PH, Ramon C, Haueisen J. Dipole models for the EEG and MEG. IEEE Trans Biomed Eng. 2002 May; 49(5):409–418. [PubMed: 12002172]

Setsompop K, Gagoski BA, Polimeni JR, Witzel T, Wedeen VJ, Wald LL. Blipped-controlled aliasing in parallel imaging for simultaneous multislice echo planar imaging with reduced g-factor penalty. Magn Res Med. 2011; 67(5):1210–1224.

Setsompop K, Kimmlingen R, Eberlein E, Witzel T, Cohen-Adad J, Mc-Nab JA, … Wald LL. Pushing the limits of in vivo diffusion MRI for the human connectome project. Neuroimage. 2013; 80(0): 220–233. [PubMed: 23707579]

Singh KD, Barnes GR, Hillebrand A, Forde EM, Williams AL. Task-related changes in cortical synchronization are spatially coincident with the hemodynamic response. Neuroimage. 2002; 16(1):103–114. [PubMed: 11969322]

Sokal, R., Rohlf, F. Biometry: The principles and practice of statistics in biological research. W. H. Freeman; 1995. Retrieved from https://books.google.com/books?id=_yZmmgEACAAJ

Sommer J, Meinhardt J, Volz HP. Combined measurement of event-related potentials EPRs and FMRI. Acta Neurobiol Exp (Wars). 2003; 63(1):49–53. [PubMed: 12784932]

Sotiropoulos SN, Moeller S, Jbabdi S, Xu J, Andersson JL, Auerbach EJ, … Lenglet C. Effects of image reconstruction on fiber orientation mapping from multichannel diffusion MRI: Reducing the noise floor using SENSE. Magn Reson Med. 2013; 70(6):1682–1689. [PubMed: 23401137]

Van Essen DC, Smith SM, Barch DM, Behrens TEJ, Yacoub E, Ugurbil K. for the WU-Minn HCP Consortium. The WU-Minn Human Connectome Project: An overview. NeuroImage. 2013; 80(C): 62–79. [PubMed: 23684880]

Van Essen DC, Ugurbil K, Auerbach E, Barch D, Behrens TE, Bucholz R, … EY. The Human Connectome Project: a data acquisition perspective. Neuroimage. 2012; 62(4):2222–2231. [PubMed: 22366334]

Vanni S, Warnking J, Delon-Martin C, Bullier J, Segebarth C. Sequence of pattern onset responses in the human visual areas: An FMRI constrained VEP source analysis. Neuroimage. 2004; 21(3): 801–817. [PubMed: 15006647]

von Ellenrieder N, Valdes-Hernandez PA, Muravchik CH. On the EEG/MEG forward problem solution for distributed cortical sources. Med Biol Eng Comput. 2009 Oct; 47(10):1083–1091. [PubMed: 19730912]

Wong CW, Olafsson V, Tal O, Liu TT. The amplitude of the resting-state fMRI global signal is related to EEG vigilance measures. Neuroimage. 2013; 83:983–990. [PubMed: 23899724]

Zotev V, Yuan H, Misaki M, Phillips R, Young KD, Feldner MT, Bodurka J. Correlation between amygdala BOLD activity and frontal EEG asymmetry during real-time fMRI neurofeedback training in patients with depression. Neuroimage Clin. 2016; 11:224–238. [PubMed: 26958462]

Appendix A: EFD summary

The information Hamiltonian $H(d, s)$ can be written (Enßlin et al., 2009) as

$$H(d,s) = H_0 - j^\dagger s + \frac{1}{2} s^\dagger D^{-1} s + H_i(d,s) \quad (8)$$

where H_0 is essentially a normalizing constant that can be ignored, D is an information propagator, j is an information source, and $\dagger$ means the complex conjugate transpose. H_i is an interaction term (Enßlin et al., 2009)

$$H_i = \sum_{n=1}^{\infty} \frac{1}{n!} \int \cdots \int \Lambda^{(n)}_{s_1 \cdots s_n} s_1 \cdots s_n ds_1 \cdots ds_n \quad (9)$$

where $\Lambda^{(n)}_{s_1 \cdots s_n}$ terms describe the interaction strength.

When the source term j, the linear information propagator D, and the nonlinear interaction terms $\Lambda^{(n)}_{s_1 \cdots s_n}$ are all known or at least some more or less accurate approximations can be used for their description, the IFT approach provides an effective, powerful, and mathematically elegant way to find an unknown signal s either by using the classical solution at the minimum of Hamiltonian ($\delta H/\delta s = 0$) or with the help of summation methods (e.g. with the help of Feynman diagrams (Feynman, 1949; Enßlin et al., 2009)).

But there is a whole class of problems where those terms are unknown and too complex for deriving effective and accurate approximations. In this case the ESP method (Frank & Galinsky, 2014), based on the principal of maximum entropy (Jaynes, 1957a, b), provides a general and effective way to introduce powerful prior information using coupling between different spatio-temporal points that is available from the data itself. This is accomplished by constructing a so called *coupling matrix* that characterizes the relation between locations i and j in the data

$$Q_{ij} = e^{-\gamma_{ij}} \quad (10)$$

Here the γ_{ij} are Lagrange multipliers that describe the relations and depend on some function of the space-time locations i and j. The eigenvalues λ_k and eigenvectors $\phi^{(k)}$ of the coupling matrix Q

$$\sum_j Q_{ij}\phi^{(k)}_j = \lambda_k \phi^{(k)}_i \quad (11)$$

then formally define the transition probability from location j to location i of the k'th mode (or path as it is often called in the random walk theory) as

$$p_{ijk} = \frac{Q_{ji}}{\lambda_k}\frac{\phi^{(k)}_i}{\phi^{(k)}_j} \quad (12)$$

For each transition matrix Eqn 12 there is a unique stationary distribution associated with each mode k:

$$\mu^{(k)} = \left[\phi^{(k)}\right]^2 \quad (13)$$

that satisfies

$$\mu_i^{(k)} = \sum_j \mu_j^{(k)} p_{ijk} \quad (14)$$

where $\mu^{(1)}$, associated with the largest eigenvalue λ_1, corresponds to the maximum entropy stationary distribution (Burda et al., 2009).

The EFD approach (Frank & Galinsky, 2016a, b) adds those coupling matrix priors into the information Hamiltonian Eqn 8 by expanding the signal s into a Fourier expansion using $\{\phi^{(k)}\}$ as the basis functions

$$s_i = \sum_k^K \left[a_k \phi_i^{(k)} + a_k^\dagger \phi_i^{\dagger,(k)} \right] \quad (15)$$

In this ESP basis the information Hamiltonian Eqn 8 can be written as

$$H(d, a_k) = -j_k^\dagger a_k + \frac{1}{2} a_k^\dagger \Lambda a_k + \sum_{n=1}^\infty \frac{1}{n!} \sum_{k_1}^K \cdots \sum_{k_n}^K \tilde{\Lambda}_{k_1 \cdots k_n}^{(n)} a_{k_1} \cdots a_{k_n} \quad (16)$$

where matrix Λ is the diagonal matrix Diag$\{\lambda_1, \ldots, \lambda_K\}$, composed of the eigenvalues of the coupling matrix, and j_k is the amplitude of kth mode in the expansion of the source j

$$j_k = \int j \phi^{(k)} ds \quad (17)$$

and the new interaction terms $\tilde{\Lambda}^{(n)}$ are

$$\tilde{\Lambda}_{k_1 \cdots k_n}^{(n)} = \int \cdots \int \Lambda_{s_1 \cdots s_n}^{(n)} \phi^{(k_1)} \cdots \phi^{(k_n)} ds_1 \cdots ds_n \quad (18)$$

For the nonlinear interaction terms $\Lambda_{s_1 \cdots s_n}^{(n)}$ the EFD method again takes coupling into account through factorization of $\Lambda^{(n)}$ in powers of the coupling matrix

$$\Lambda_{s_1 \cdots s_n}^{(n)} = \frac{\alpha^{(n)}}{n} \sum_{p=1}^n \prod_{\substack{m=1 \\ m \neq p}}^n Q_{pm} \quad (19)$$

where $\alpha^{(n)} \lesssim 1/\max\ (j_k^n/\lambda_k)$, which results in

$$\widetilde{\Lambda}^{(n)}_{k_1\cdots k_n} = \frac{\alpha^{(n)}}{n}\sum_{p=1}^{n}\left(\frac{1}{\lambda_{k_p}}\prod_{m=1}^{n}\lambda_{k_m}\right)\int\left(\prod_{r=1}^{n}\phi^{k_r}\right)ds \quad (20)$$

Thus the EFD approach provides a very simple expression for the classical solution for the amplitudes a_k

$$\Lambda a_k = \left(j_k - \sum_{n=1}^{\infty}\frac{1}{n!}\sum_{k_1}^{K}\cdots\sum_{k_n}^{K}\widetilde{\Lambda}^{(n+1)}_{kk_1\cdots k_n}a_{k_1}\cdots a_{k_n}\right) \quad (21)$$

through the eigenvalues and eigenvectors of coupling matrix (that may also include some noise corrections (Frank & Galinsky, 2016a, b)).

Appendix B: Coupling for different modalities

For the HRA dataset we define a simple intensity weighted nearest neighbors coupling matrix as

$$Q^H_{ij} = e^{-\gamma_{ij}} = \begin{cases} d^H_i d^H_j & \text{nearest neighbors} \\ 0 & \text{not connected} \end{cases} \quad (22)$$

For DWI data, the GO-ESP procedure uses the spin density function $G(\boldsymbol{r}, \boldsymbol{R})$ expressed with the help of the spherical wave decomposition as

$$G(\boldsymbol{r},\boldsymbol{R}) = 4\pi\sum_{l=0}^{\infty}\sum_{m=-l}^{l} i^l Y_l^m(\widehat{\boldsymbol{R}})g_{lm}(\boldsymbol{r},R), \quad (23)$$

$$g_{lm}(\boldsymbol{r},R) = \int W(\boldsymbol{r},\boldsymbol{q})j_l(qR)Y_l^{m\,*}(\widehat{\boldsymbol{q}})d\boldsymbol{q}\,. \quad (24)$$

and generate the symmetrized scale dependent coupling matrix Q^D_{ij} as

$$Q^D_{ij}(\ell) = Q^D_{ji}(\ell) = \frac{1}{2}\left[G\left(\boldsymbol{r}_i, (\boldsymbol{r}_i - \boldsymbol{r}_j)\ell\right) + G\left(\boldsymbol{r}_j, (\boldsymbol{r}_j - \boldsymbol{r}_i)\ell\right)\right], \quad (25)$$

where ℓ represents the dimensionless ratio of scales of dynamic displacement $\boldsymbol{R}$ to the spatial (voxel) scales $\boldsymbol{r}$, $j_l(qR)$ is the spherical Bessel function of order l and $Y^m_l(\hat{\boldsymbol{q}}) = Y^m_l(\Omega_{\hat{\boldsymbol{q}}}) = Y^m_l(\theta_q, \phi_q)$ is the spherical harmonic with θ_q and ϕ_q being the polar and azimuthal angles of the vector $\boldsymbol{q}$, and similarly for the vector $\boldsymbol{R}$, and $W(\boldsymbol{r}, \boldsymbol{q})$ is the DW1 signal (see Galinsky & Frank (2015) for more details).

For rsFMRI the EFD procedure employs the frequency ω dependent spatial coupling matrix $Q^F_{ij}(\omega)$ as

$$Q^F_{ij}(\omega_0) = \mathcal{R}^n_{ij} d^F_i(\omega_0) d^F_j(\omega_0), \quad (26)$$

$$Q^F_{ij}(\omega_l) = \mathcal{R}^n_{ij}\left(\phi^{(1)}_i(\omega_0) d^F_j(\omega_l) + \phi^{(1)}_j(\omega_0) d^F_i(\omega_l)\right), \quad (27)$$

here $d^F_i(\omega)$ is the temporal Fourier mode of the rsFMRI data d^F with the frequency ω, $\phi^{(1)}_i(\omega_0)$ is the eigenvector of $Q^F(\omega_0)$ that corresponds to the largest eigenvalue, and $\mathcal{R}_{ij}$ can include some function of the pair correlations taken to the nth power, for example a simple mean of the pair correlations, that is equivalent to a product of signal means ($\bar{d}^F$) for a periodic signal

$$\mathcal{R}_{ij} = \frac{1}{T}\int_0^T C_{ij}(t)dt \equiv T\bar{d}^F_i \bar{d}^F_j \quad (28)$$

or a maximum correlation of mean subtracted signal

$$\mathcal{R}_{ij} = \max_{0 \le t \le T} \mid C_{ij}(t) - T\bar{d}^F_i \bar{d}^F_j \mid \quad (29)$$

where $C_{ij}(t)$ is the pair correlation

$$C_{ij}(t) \equiv \int d^F_i(t-\tau) d^F_j(\tau) d\tau \quad (30)$$

The EFD procedure can then be extended to incorporate information from all of the modalities simultaneously by incorporating these single modality coupling matrices Q_{ij}^{H}, Q_{ij}^{D} and Q_{ij}^{F} in Eqn 31 to generate the intermodality coupling matrix $\mathcal{Q}_{ij}$.

Appendix C: JESTER summary

Assuming that we have $m = 1, \ldots, M$ different modalities $d^{(\mathrm{m})}$ with the coupling matrices $Q^{(\mathrm{m})}$ that all correspond to the same unknown signal s, than we can construct an intermodality coupling matrix as the product of these coupling matrices for the individual modalities expressed in the ESP basis and registered to a common reference frame, which we denote $\tilde{Q}^{(\mathrm{m})}$: That is, the joint coupling matrix is $\mathcal{Q}^{(\mathrm{m})} = \Pi_m \tilde{Q}^{(\mathrm{m})}$. More specifically, the joint coupling matrix $\mathcal{Q}_{ij}$ between any two space-time locations (i, j) can be written in the general (equivalent) form as

$$\ln \mathcal{Q}_{ij} = \sum_{m=1}^{M} \beta_{ij}^{(m)} \ln \tilde{Q}_{ij}^{(m)} \quad (31)$$

where the exponents $\beta^{(\mathrm{m})}$ can either be some constants or functions of data collected for different modalities

$$\beta_{ij}^{(m)} \equiv \beta^{(m)}(\tilde{\boldsymbol{d}}_i, \tilde{\boldsymbol{d}}_j), \quad \tilde{\boldsymbol{d}}_i \equiv \{\tilde{d}_i^{(1)}, \ldots, \tilde{d}_i^{(M)}\} \quad (32)$$

$\tilde{d}_i^{(m)}$ and $\tilde{Q}_{ij}^{(m)}$ represent, respectively, the data and the coupling matrix of the modality dataset m represented in the ESP basis and evaluated at locations r_i and r_j of a common reference domain R:

$$\tilde{d}_i^{(m)} = d^{(m)}\left(\psi^{(m)}(r_i)\right), \quad \tilde{Q}_{ij}^{(m)} = Q^{(m)}\left(\psi^{(m)}(r_i), \psi^{(m)}(r_j)\right) \quad (33)$$

where $\psi^{(\mathrm{m})} : R \rightarrow X$ denotes a diffeomorphic mapping of m-th modality from the reference domain R to an acquisition space X.

EEG/MEG addition to JESTER employs the frequency ω dependent spatial coupling matrix $Q_{ij}^{E}(\omega)$, that is similar to rsFMRI, as

$$Q_{ij}^{E}(\omega_0) = \mathcal{R}_{ij}^{n} d_i^{F}(\omega_0) d_j^{E}(\omega_0), \quad (34)$$

$$Q_{ij}^{E}(\omega_l) = \mathcal{R}_{ij}^{n}\left(\xi_i^{(1)}(\omega_0)d_j^{E}(\omega_l) + \xi_j^{(1)}(\omega_0)d_i^{E}(\omega_l)\right), \quad (35)$$

here $d_i^E(\omega)$ is the temporal Fourier mode of the EEG/MEG data d^E with the frequency ω, $\xi_i^{(1)}(\omega_0)$ is the eigenvector of $Q^E(\omega_0)$ that corresponds to the largest eigenvalue, and $\mathcal{R}_{ij}$ can include some function of the pair correlations taken to the nth power, for example a simple mean of the pair correlations, that is equivalent to a product of signal means ($\bar{d}^E$) for a periodic signal

$$\mathcal{R}_{ij} = \frac{1}{T}\int_0^T C_{ij}(t)dt \equiv T\bar{d}_i^E\bar{d}_j^E \quad (36)$$

or a maximum correlation of mean subtracted signal

$$\mathcal{R}_{ij} = \max_{0 \le t \le T} \mid C_{ij}(t) - T\bar{d}_i^E\bar{d}_j^E \mid \quad (37)$$

where $C_{ij}(t)$ is the pair correlations

$$C_{ij}(t) \equiv \int d_i^E(t-\tau)d_j^E(\tau)d\tau \quad (38)$$

Appendix: Video links for figure 1

- Top–Left: http://abeta.ucsd.edu/Videos.git/fmri2eeg/eeg-1-2-b.mp4
- Top–Right: http://abeta.ucsd.edu/Videos.git/fmri2eeg/eeg-1-3-b.mp4
- Bottom–Left: http://abeta.ucsd.edu/Videos.git/fmri2eeg/eeg-2-3-b.mp4
- Bottom–Right: http://abeta.ucsd.edu/Videos.git/fmri2eeg/eeg-3-4-b.mp4

Appendix: Video links for figure 2

- Top–Left: http://abeta.ucsd.edu/Videos.git/fmri2eeg/eeg-1-2-i.mp4
- Top–Right: http://abeta.ucsd.edu/Videos.git/fmri2eeg/eeg-1-3-i.mp4
- Bottom–Left: http://abeta.ucsd.edu/Videos.git/fmri2eeg/eeg-2-3-i.mp4
- Bottom–Right: http://abeta.ucsd.edu/Videos.git/fmri2eeg/eeg-3-4-i.mp4

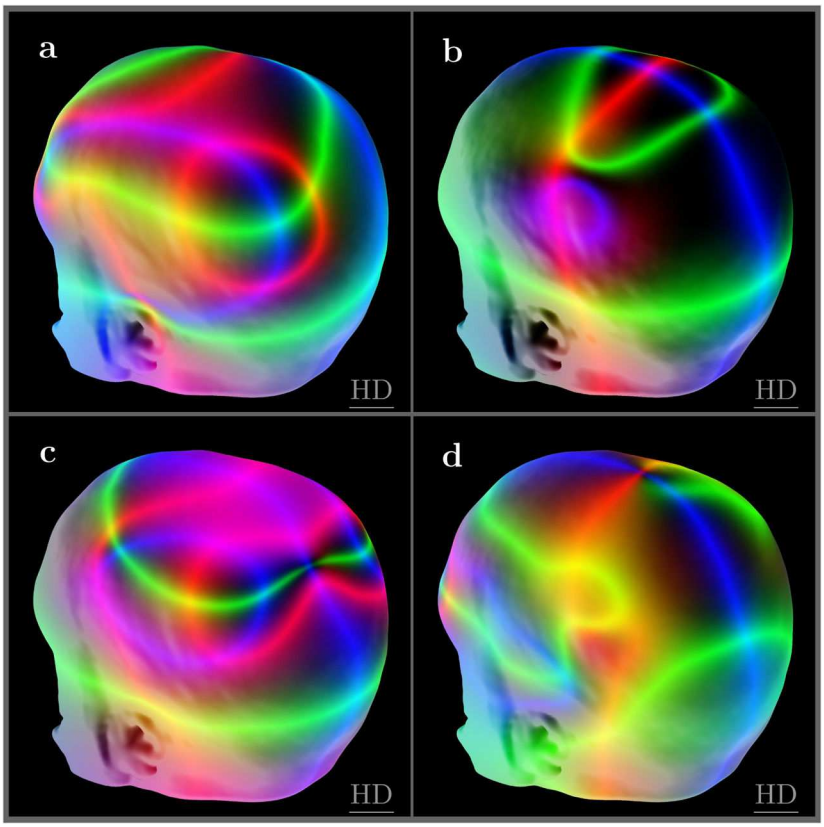

Figure 1.
Several time shots of skull electric field distributions produced by different FMRI functional modes estimated using JESTER.

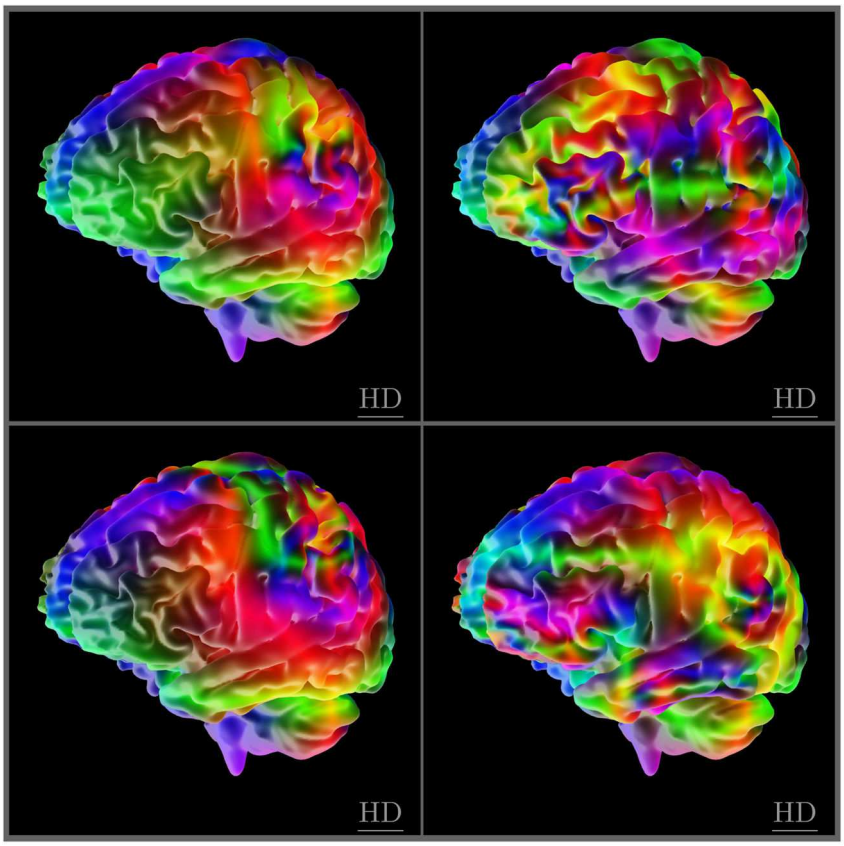

Figure 2.
Several time shots of brain electric field distributions produced by the same FMRI functional modes as in Figure 1 estimated using JESTER.

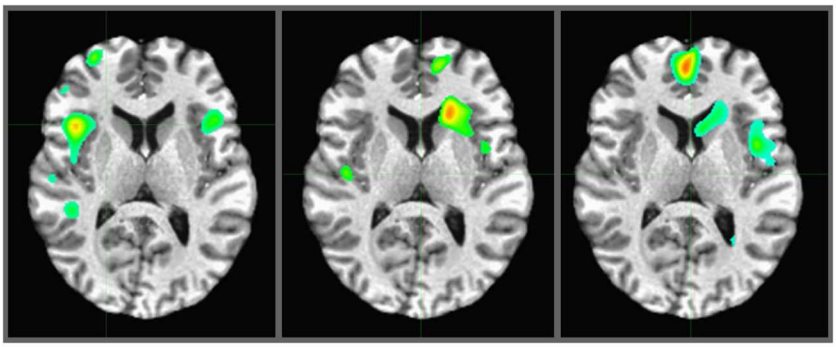

Figure 3.
Demonstration of activation modes created from MEG data using JESTER and constrained by high resolution anatomical MRI data. Activated regions are (left) bilateral anterior insula, which is among the most common activation patterns in rsFMRI, (middle) right caudate, and (right) medial frontal gyrus.

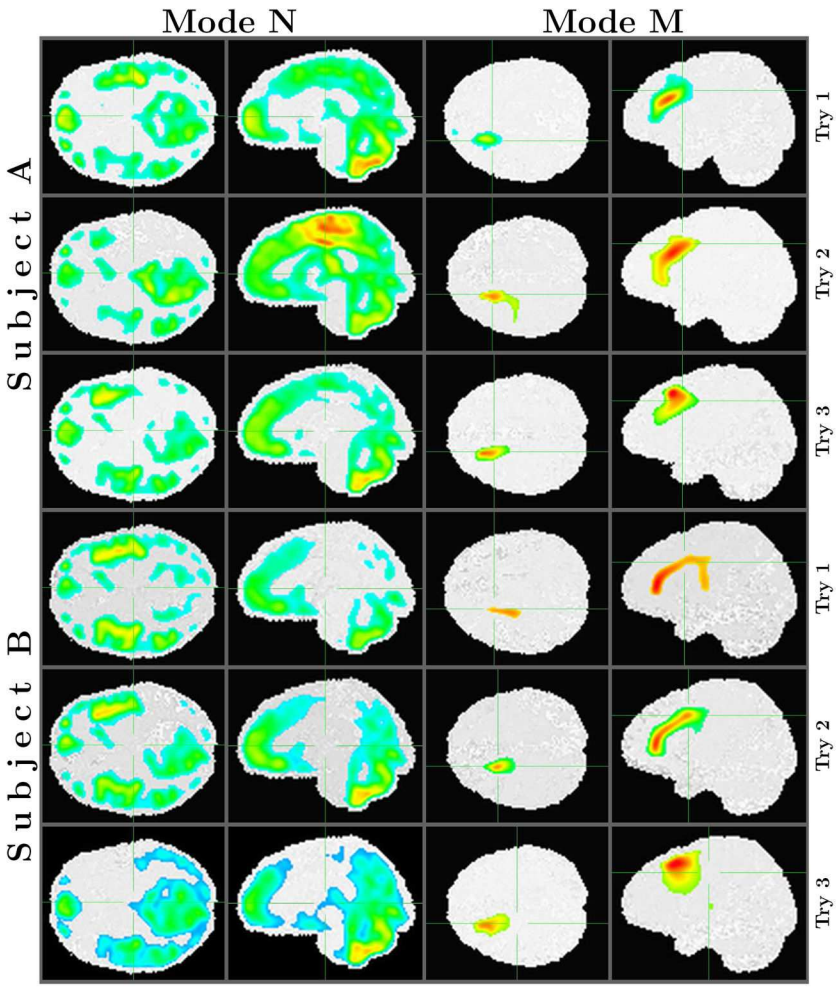

Figure 4.

EEG functional modes detected from volumes generated by CORT-JESTER. The modes display excellent repeatability between sessions, with the intraclass correlation coefficient (Sokal & Rohlf, 1995) (ICC) equals to 0.9985, but at the same time provide noticeable subject differences. The modes were generated with the same spatio-temporal resolution as was used for FMRI acquisition (2mm × 2mm × 2mm × 2s and 80 × 95 × 75 voxels with 237 time points).

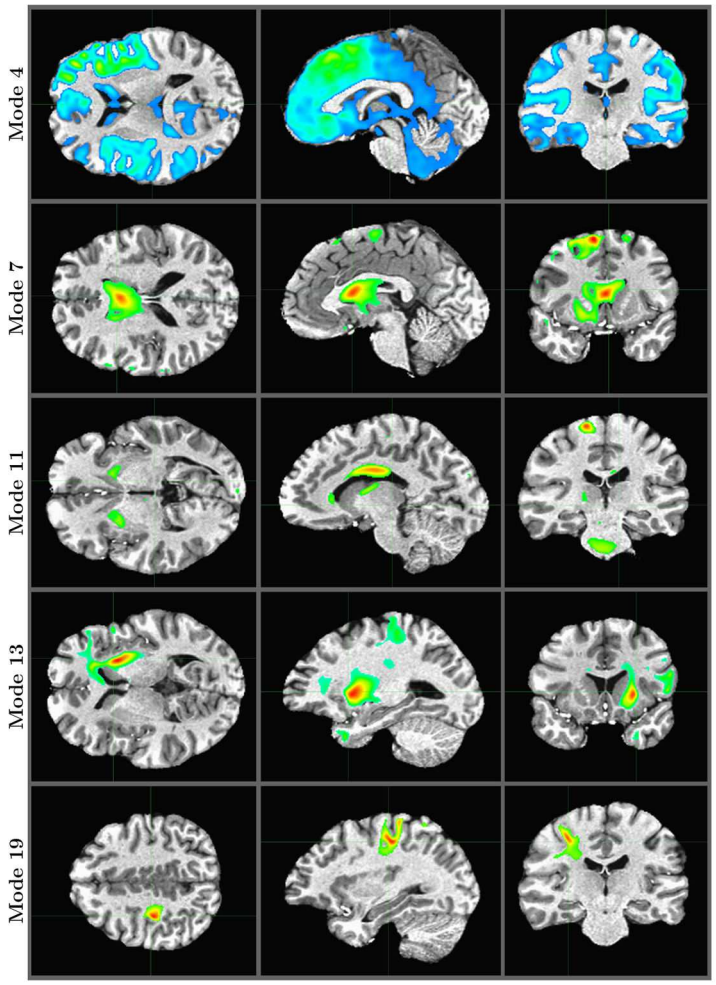

Figure 5.
Resting state EEG functional modes generated for alpha band using HRA spatial resolution (1mm×1mm×1mm and 161×191×151 voxels).

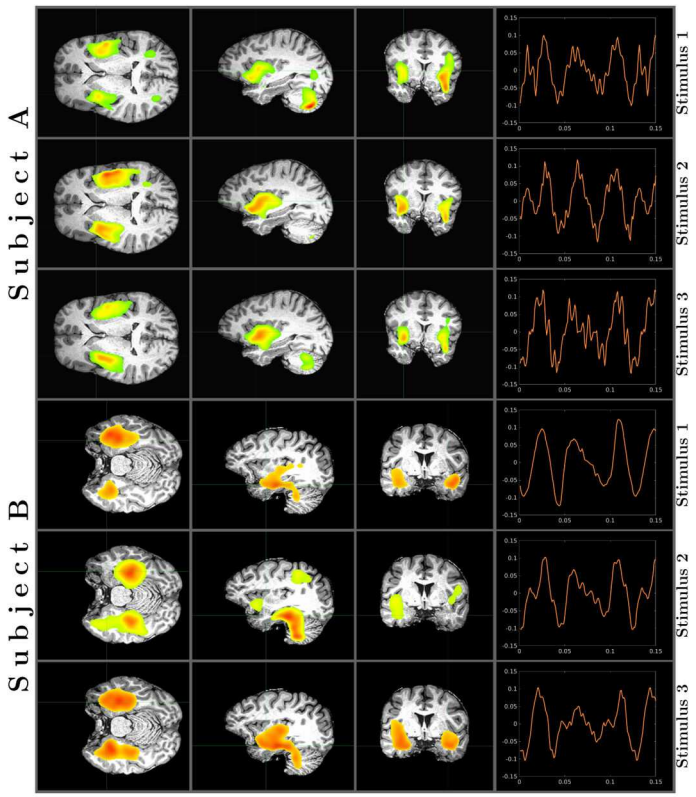

Figure 6.

Task based EEG functional modes generated by CORT-JESTER for two subjects using alpha EEG band. The first three columns show three spatial projections, the fourth column shows a temporal course (using seconds for the duration units and arbitrary normalization for the amplitude). The modes show very good similarity between similar stimuli in each subject.

Table 1

The dielectric properties for brain tissues at 10Hz frequency. The dielectric parameters are based on the Gabriel dispersion relationships (Gabriel et al., 1996b, a). The tissue permittivities are shown normalized by the permittivity of vacuum $\varepsilon_0 = 8.854187817\times10^{-12}$ F/m.

Tissue	Source	Permittivity	Conductivity (S/m)
Grey Matter	Grey Matter	4.07E+7	2.75E-2
White Matter	White Matter	2.76E+7	2.77E-2
Cerebrospinal Fluid	Cerebrospinal Fluid	1.09E+2	2.00E+0
Skull Cancellous	Bone Cancellous	1.00E+7	7.56E-2
Skull Cortical	Bone Cortical	5.52E+4	2.00E-2
Skin	Skin (Dry)	1.14E+3	2.00E-4